

Design and Thermal Behavior Analysis of a Plan Air Solar Collector

Salmwende Eloi Tiendrebeogo^{1,2,*}, Tubreoumya Guy Christian¹, Kafando Guetinsom Jean¹, Nana Bernard^{1,2}, Kere Moumini², Dissa Alfa Oumar¹, Koulidiati Jean¹, Bere Antoine¹

¹Environmental Physics and Chemistry Laboratory (LPCE), University of Joseph KI - ZERBO, Ouagadougou, Burkina Faso

²Environment Department, Ecole Normale Supérieure (ENS), Ouagadougou, Burkina Faso

Email address:

tiendrebeogoeloi@yahoo.fr (S. E. Tiendrebeogo)

*Corresponding author

To cite this article:

Salmwende Eloi Tiendrebeogo, Tubreoumya Guy Christian, Kafando Guetinsom Jean, Nana Bernard, Kere Moumini, Dissa Alfa Oumar, Koulidiati Jean, Bere Antoine. Design and Thermal Behavior Analysis of a Plan Air Solar Collector. *Science Journal of Energy Engineering*. Vol. 10, No. 1, 2022, pp. 1-7. doi: 10.11648/j.sjee.20221001.11

Received: January 8, 2022; **Accepted:** January 25, 2022; **Published:** February 16, 2022

Abstract: In order to find heat production techniques for drying and heating applications of premises in tropical climates from process characterization studies, a flat air collector with air and forced convection was first designed. A simulation of solar radiation, thermal behavior of the solar collector and an experimental test of the latter were carried for validation. The time profiles of the evolution of solar radiation and the temperatures of the heat transfer fluid at the inlet and outlet of the collector as well as those of the collector components during a day were presented, November 17th, 2019. During this day, for an ambient air temperature at the collector inlet varying between 20°C and 41°C, the experimental temperatures of the absorber and solar collector outlet air temperature are respectively 96°C and 78°C for maximum measured solar irradiation of the order of 900 W/m². For the same interval of variation of ambient air temperature, the simulated temperatures of the absorber and of the solar collector outlet air are respectively of the order of 105°C and 90°C when the simulated maximum solar irradiation attains 880 W/m² of collection at true solar noon. The values of R² obtained for the data of the solar radiation, collector outlet air temperature and temperatures of the absorber are respectively of the order of 0.960, 0.98 and 0.950, indicating a good correlation between the experimental and predicted data; whereas the root mean square error (RMSE) are respectively around 0.020, 0.013 and 0.011, showing a very good match between experimental and modelled temperatures. The temperature range at the outlet of the present device which is simple and achievable at low cost is important for the drying needs of the various products and heating.

Keywords: Design, Solar Collector, Radiation, Temperature, Simulation, Experience

1. Introduction

In a context of socio-economic and energy fragility, health insecurity and the absence of efficient processes that link innovation to the promotion of heat production systems, it is high time to focus on the resilience of communities with pay attention to the green alternative. Like the Sahelian countries, Burkina Faso is a country with high solar potential due to its geographic position. Average daily sunshine is estimated at 5.5 kWh/m² per year [1]. It is a country with high agricultural potential with around 86% of the working population where the economy is mainly based. To reduce the waste of agricultural products, some products are dried using

traditional techniques. There are modern technical means of producing heat for drying needs but which are energy-consuming and less accessible to rural communities. In the literature, the use conditions of solar thermal energy varied greatly from one region to another [2, 3]. Several research works [4-7] carried out on thermal solar collectors made of suitable materials have found that in real climates, these collectors provide a temperature of the order of 70°C, which is important for heating. Water and drying of fruits and vegetables. However, this temperature range is lower for some processes, especially in modern manufacturing industries.

Despite these achievements and progress, the control of solar heat production, the inaccessibility of adequate equipment at low cost and the optimization of operation remain the main challenges to be met. The general objective of this work is to develop a flat air solar collector intended for the drying of agro-food and fishery products. It's about developing a flat air solar collector, to experimentally measure the solar irradiation and the temperatures of the collector components and to simulate the evolution of these characteristic parameters by modeling material transfers in dynamic regime. The originality of this study lies in the integration of a plate with rectangular fins of thickness 2 mm and parallel to the direction of flow of the heat transfer fluid on the internal face of the rear insulation and taking into account of true solar time in modeling.

2. Materials and Methods

2.1. Design

2.1.1. Choice of Materials

Three main criteria guided the choice of materials to be used for the manufacture of dryer: the availability of local material, the acceptable cost and the viable thermal properties. The main materials used are: the absorber made of corrugated aluminum sheet; the transparent cover in clear glass and the polystyrene insulation.

2.1.2. Physical Properties and Assembly Steps

The dimensions and physical properties of the elements of this collector are listed in table 1. The different stages of mounting the device are presented below (see Figure 1).

Table 1. Dimensions and physical properties of the collector components.

Physical characteristics	Collector	Glass	Absorber	Rear insulation	Lateral insulation	Lateral insulation
Thickness [m]	---	0.004	0.002	0.150	0.150	---
Length [m]	1.940	1.900	1.900	1.900	1.900	1.900
Width [m]	0.840	0.800	0.800	0.800	0.800	0.800
Volumic mass [kg / m^3]	---	2700	2700	12	12	7800
Specific heat [$\text{J} / \text{kg.K}$]	---	834	880	1300	1300	460
Thermal conductivity [$\text{W} / \text{m.K}$]	---	0.800	---	0.040	0.040	40



(a)

(b)



(c)

(d)

Figure 1. Main steps in mounting of collector: (a) Realization of the framework and insulation of the walls with polystyrene. (b) Installation of the finned plate on the internal face of the rear insulation. (c) Installation of the absorber: corrugated Al sheet painted matt black. (d) Installation of the glass and sealing of the seals with silicone.

2.2. Experimentation

2.2.1. Device and Operation

The ambient air is first captured from the outside through the rectangular vein using a suction fan (extractor) supplied by a PV plate. The air-absorber contact as well as the convective transfer generates inside the collector (see Figure 2) an increase an increase collector outlet air temperature until some value. This phenomenon depends on the sunshine and the properties of the device [8, 9].



Figure 2. Experimental device. (1) Collector, (2) Enter air, (3) Glass, and (4) Extractor.

2.2.2. Parameters and Measuring Devices

The global solar irradiation that falls on the collector (W/m^2) is measured using a solarimeter (Figure 3). The solarimeter is

connected to a Midi brand datalogger (Figure 5). The overall radiation received on the flat surface of the absorber (G) in W/m^2 can easily be calculated by multiplying the signal of the outlet voltage U_s (in mV) by the nominal sensitivity of the device ($13.33 W/m^2.mV$) as indicated by the relation $G = 13.330 * U_s$. Every 10 minutes, temperatures are measured using type K thermocouples connected to datalogger Midi logger brand with an accuracy of $\pm 0.050\%$ of the value read $+1^\circ C$ pour $-100^\circ C < T \leq 1370^\circ C$. The thermocouples are placed at the inlet, at the outlet of the collector, on the absorber, on the fin plate and on the internal face of the glass. The results are displayed and saved through the Midi brand datalogger (Figure 4). The wind speed was measured by an anemometer (Figure 5). All the experiments carried out on the collector were carried out with an average flow of $0.013 kg/s$.



Figure 3. Solarimeter.



Figure 4. Midi brand datalogger.



Figure 5. Anemometer.

2.3. Modeling and Simulation

2.3.1. Assumptions and Equivalent Diagram

For our study in variable basing regime based on the equivalent diagram (see Figure 6), the following assumptions are made:

- 1) the flow is unidirectional and the regime is assumed to be transient,
- 2) the parameters are homogeneous on a section of the collector perpendicular to the flow,
- 3) the sky and the glass are assimilated respectively to black and gray bodies,
- 4) the ambient temperature is uniform around the collector,
- 5) the physical properties of the materials used are constant,
- 6) pressure losses and viscosity effects in heat transfer fluid are negligible,
- 7) the effects of dust and dirt on the glass are negligible,
- 8) the coefficient of exchange by convection between the heat transfer fluid and the absorber is the same as that between the heat transfer fluid and the finned plate,
- 9) the convection exchange coefficient between the confined air and the absorber is the same as that between the confined air and the internal face of the glass.

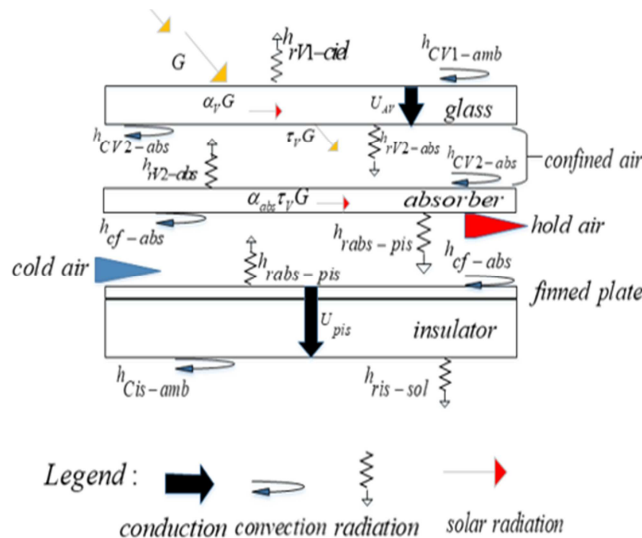


Figure 6. Equivalent diagram and transfer mechanisms.

2.3.2. Balance Transfer Equations for Materials

In the network of Figure 6, each component represents a

part of the dryer symbolized by its temperature. On this network, the thermal resistances, the heat capacities, the

evaporating flux and the thermal losses were also as:
represented. The energy balance on each node was written

External face of the glass

$$\rho_V C p_V V_V \frac{\partial T_{V1}}{\partial t} = [\alpha_V G S_V + h_{rv-ciel} S_V (T_{ciel} - T_{V1}) + h_{cv-amb} S_V (T_{amb} - T_{V1}) + U_{AV} S_V (T_{V2} - T_{V1})] \quad (1)$$

Internal face of the glass

$$\rho_V C p_V V_V \frac{\partial T_{V2}}{\partial t} = [h_{cv-as} S_V (T_{as} - T_{V2}) + h_{rv-abs} S_V (T_{abs} - T_{V2}) + U_{AV} S_V (T_{V1} - T_{V2})] \quad (2)$$

The absorber

$$\rho_{abs} C p_{abs} V_{abs} \frac{\partial T_{abs}}{\partial t} = \left[\alpha_{abs} \tau_V G S_{abs} + h_{rv-abs} S_{abs} (T_{V2} - T_{abs}) + h_{ris-abs} S_{abs} (T_{pis} - T_{abs}) + h_{cv-as} S_{abs} (T_{as} - T_{abs}) + h_{cf-abs} S_{abs} (T_f - T_{abs}) \right] \quad (3)$$

For the heat transfer fluid

$$\rho_f C p_f V_f \frac{\partial T_f}{\partial t} = [h_{cf-abs} S_{abs} (T_{abs} - T_f) + h_{cf-abs} S_{pis} (T_{pis} - T_f)] \quad (4)$$

Finned plate placed on the internal face of the insulation are confused

$$\rho_{pis} C p_{pis} V_{pis} \frac{\partial T_{pis}}{\partial t} = [h_{rabs-pis} S_{pis} (T_{abs} - T_{pis}) + h_{cf-pis} S_{pis} (T_f - T_{pis}) + U_{pis} S_{pis} (T_{eis} - T_{pis})] \quad (5)$$

External face of the insulation

$$\rho_{is} C p_{is} V_{is} \frac{\partial T_{eis}}{\partial t} = [h_{rsol-is} S_{is} (T_{sol} - T_{eis}) + h_{camb-is} S_{is} (T_{amb} - T_{eis}) + U_{pis} S_{is} (T_{pis} - T_{eis})] \quad (6)$$

i. Expressions of transfer coefficients

The use of radiative and convective exchange coefficients simplifies the mathematical formulation of the heat transfer equations. The modes of exchange taking

place in collector are; convective, radiative and conduction. The transfer coefficients (Table 2) are drawn up considering the architecture and the flow mode of the fluid [10-12].

Table 2. Thermophysical properties of air used in model solutions.

Transfer coefficient	Relations
Glass and sky	$h_{rv-ciel} = \sigma(T_V^2 + T_{ciel}^2)(T_V + T_{ciel})$ or $T_{ciel} = 0.0552 * T_{amb}^{1.5}$
Insulation and floor	$h_{ris-sol} = \sigma(T_{is}^2 + T_{sol}^2)(T_{is} + T_{sol})$ with $T_{sol} = T_{amb} + 2$
Absorber and window	$h_{rv-abs} = \sigma(T_{V2}^2 + T_{abs}^2)(T_{V2} + T_{abs}) / (\epsilon_{abs}^{-1} + \epsilon_V^{-1} - 1)$
Absorber and finned plate	$h_{rpis-abs} = \sigma(T_{pis}^2 + T_{abs}^2)(T_{pis} + T_{abs}) / (\epsilon_{abs}^{-1} + \frac{(\epsilon_V^{-1} - 1) * S_{abs}}{(S_{pis} + n * S_a)})$
Glass and ambient air	$h_{cv-amb} = h_{cis-amb} = 5.7 + 3.8 * V_{vent}$
Glass, absorber and static air	$h_{cv-abs} = h_{cabs-v} = Nu * \lambda_{air} / D_H$ $Nu = [0.06 - 1.17](\beta / 90) * Gr^{1/3}$ $Gr = g \Delta T e_1^3 / \nu_{air}^2 T_{amb}$
Absorber and heat transfer fluid	$h_{cabs-f} = h_{cis-f} = Nu * \lambda_{air} / D_{H2}$ $D_{H2} = 4 L_{eoc} / 2(L + e_{oc})$ $Nu = 0.0158 Re^{1.8}$; $Re = V_{air} D_{H2} / \lambda_{air}$

ii. Thermal losses from the collector

One of the originality of the modeling resides in the taking into account of the heat losses between the various constituents of the solar collector as well as with the ambient environment. By negating the losses through the side walls, we are left with two cases of significant losses which are:

losses towards the front and rear. These overall losses per square meter of catchment area are represented by the equation [13].

$$Q_T = U_T (T_{abs} - T_{amb}) \text{ with } U_T = U_{avant} + U_{back} \quad (8)$$

$$U_{\text{avant}} = 1 / \left[(h_{\text{rv-ciel}} + h_{\text{cv-amb}})^{-1} + U_{\text{av}}^{-1} + (h_{\text{rv-abs}} + h_{\text{cv-abs}})^{-1} \right] \quad (9)$$

$$U_{\text{back}} = 1 / \left[U_{\text{pis}}^{-1} + (h_{\text{ris-sol}} + h_{\text{cis-amb}})^{-1} \right] \quad (10)$$

G : Global solar power $[W / m^2]$; h_C : Convective exchange coefficient $[W / m^2.K]$, h_r : Radiative exchange coefficient $[W / m^2.K]$; U : Conductive transfer coefficient; α , ε , τ , ρ : Absorption, emissivity, transmission and reflection coefficients.

$$K_2 = f(t_i + \frac{h}{2}, y_i + \frac{h \cdot K_1}{2}) ; K_3 = f(t_i + \frac{h}{2}, y_i + \frac{h \cdot K_2}{2}) ; K_4 = f(t_i + h, y_i + h \cdot K_3) \text{ With } y_{i+1} = y_i + \frac{1}{6}(K_1 + 2 \cdot K_2 + 2 \cdot K_3 + K_4) ; h = t_{i+1} - t_i \quad (18)$$

Furthermore, the accuracy in the determination of experimental results is estimated the statistical parameters: the coefficient and the root mean square error (RMSE). These parameters were expressed according to the following equations which was solved by multi-linear regression analysis [14].

$$RMSE = \sqrt{\frac{\sum_{z=1}^N (Y_{\text{exp},z} - Y_{\text{pre},z})^2}{\sum_{z=1}^N (\bar{Y}_{\text{exp},z} - Y_{\text{pre},z})^2}} \quad (12)$$

$$R^2 = 1 - \frac{\sum_{z=1}^N (Y_{\text{exp},z} - Y_{\text{pre},z})^2}{\sum_{z=1}^N (\bar{Y}_{\text{exp},z} - Y_{\text{pre},z})^2} \quad (13)$$

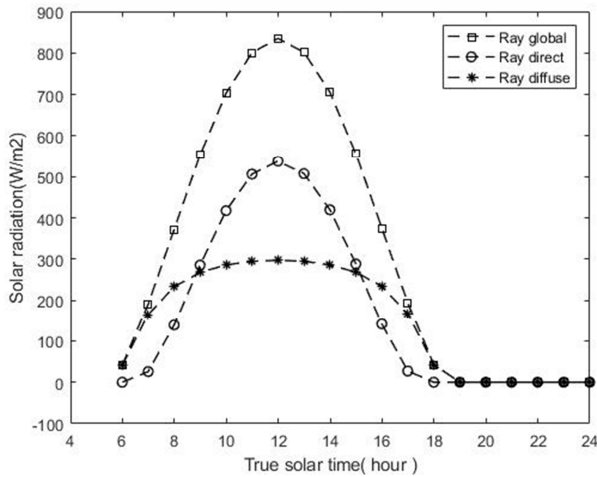


Figure 7. Experimental curve of direct, diffuse and global solar radiation.

3. Results and Discussion

3.1. Experimental Results

3.1.1. Temporal Variation of Experimental Solar Radiation

It is shown in Figure 7, the evolution of direct, diffuse and global solar radiation measured during the experimental

iii. Simulation of transfers

The equations transfer system has been solved by the Runge-Kutta methods which are numerical approximation methods of solution of the differential equations. The Runge-Kutta method of order 4 (RK4) is very commonly used for solving ordinary differential equations (ODE) and very stable for the common functions of physics. The RK4 method is derived from the Euler method, it uses three intermediate points to progress from the point (t_i, y_i) on point (t_{i+1}, y_{i+1}) based on the following functions.

$$K_1 = f(t_i, y_i) ; \quad (11)$$

day of November 17th, 2019. The solar radiation evolves gradually from sunrise, reaches a maximum value of the order of 900 W.m-2 at true solar noon (12 noon) then decreases rapidly to cancel out at sunset time. Between 9 hour and 15 hour, we notice the direct radiation is higher than the diffuse one because of strong sunshine during this period.

3.1.2. Temporal Variation of the Temperatures of the Collector Components, of the Heat Transfer Fluid (Air) at the Inlet and Outlet of the Collector

It is shown in Figure 8 the temporal variations in experimental temperatures of the internal face of the glass, of the absorber, of the finned plate placed on the internal face of the rear insulator of the collector, of the ambient air, of the air at the inlet and outlet of the collector. We see that all temperatures have an inflection point. From the beginning, the temperatures increase until around 12 hours (True Solar Noon) then decrease rapidly just after this period. At any time between 8 hours and 6 hours, the temporal temperatures of the absorber, of the internal face of the glass, of the collector outlet air are the highest. They are followed by that of the finned plate, the air at the inlet. The temperatures maximum values of: absorber, internal face of the glass, collector outlet air, finned plate, air inlet are respectively 96°C, 80°C, 78°C, 65°C and 40°C. The maximum value of the difference in air temperature between the outlet and the inlet of the collector is of the order of 38°C for a maximum irradiation of 900 W/m² (Figure 8). This temperature increment is greater than that observed (30°C) under the same climatic conditions by Compaore A et al., 2018 [15]. The difference in air temperature between the inlet and the outlet across any solar collector reflects the thermal energy available for drying. We note that close to sunset, the absorber cools faster than the fin plate and the heat transfer fluid to the benefit of the latter (see Figure 8) because of its low thermal inertia. In view of the maximum temperature difference recorded during the test of this collector (38°C) we can say that the developed collector is valid for drying applications.

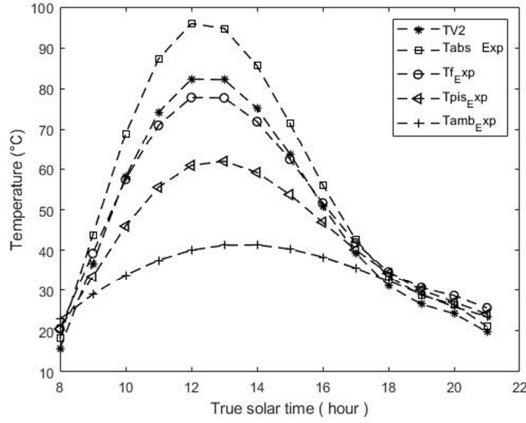


Figure 8. Experimental curves of the temperatures of the collector components, outlet air and inlet.

3.2. Comparison of Experimental and Simulated Curves

The mathematical model that we established on the basis of the energy balances predicts the evolution of the account of the dynamic behavior of the plane air collector with single pass. These results are validated by the experimental tests presented above.

3.2.1. Comparison of Experimental and Simulated Results of Solar Radiation

In Figure 9, a comparison of experimental and simulated curves of solar radiation is presented. We note that the two curves have the same behavior and that the experimental curve remains below the theoretical curve. They reach their maximum values around 12 hours. This small difference observed is explained by the presence of obstacles including the presence of clouds, shade of trees and the house. Given the small difference between these two curves, we can say that the proposed solar radiation model satisfactorily predicts the evolution of solar radiation.

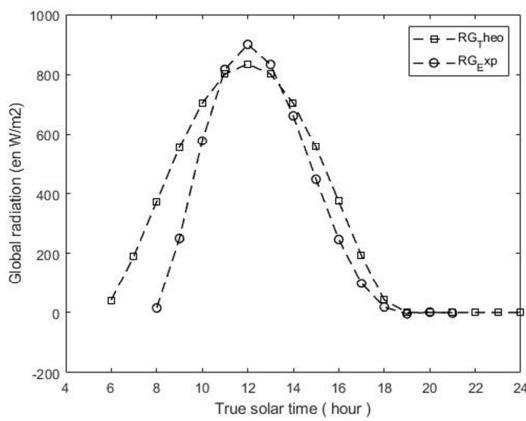


Figure 9. Comparison of experimental and simulated curves of solar radiation.

3.2.2. Comparison of Experimental and Simulated Solar Collector Outlet Air Temperature

It is compared in Figure. 10, the time curves of experimental and simulated solar collector outlet air temperature. We notice that the curves have a similar shape.

The simulated collector outlet air temperature remains slightly higher than that measured from sunrise to sunset. They reach the respective maximum values of around 80°C and 90°C. This minor deviation is due to the variable operating conditions of the parameters of solar radiation, inlet air temperature and wind speed observed in Figure 9.

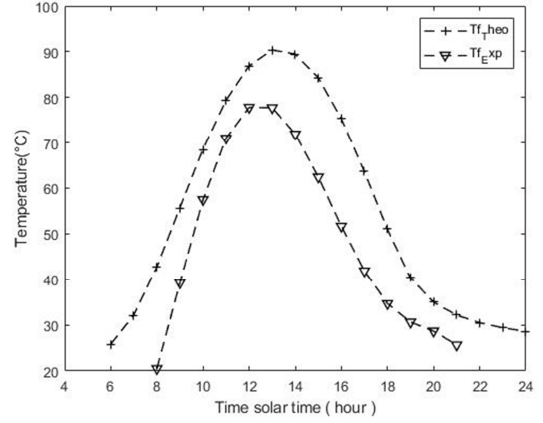


Figure 10. Comparison of experimental and simulated collector outlet air temperatures curves.

3.2.3. Comparison of Experimental and Simulated Absorber Temperature Curve

In Figure 11, we present the comparison of the experimental and simulated absorber temperature curve. In this figure we also see that the simulated absorber temperature remains slightly higher than that measured from sunrise to sunset. This difference is due to that observed between simulated and experimental solar radiation (see Figure 9).

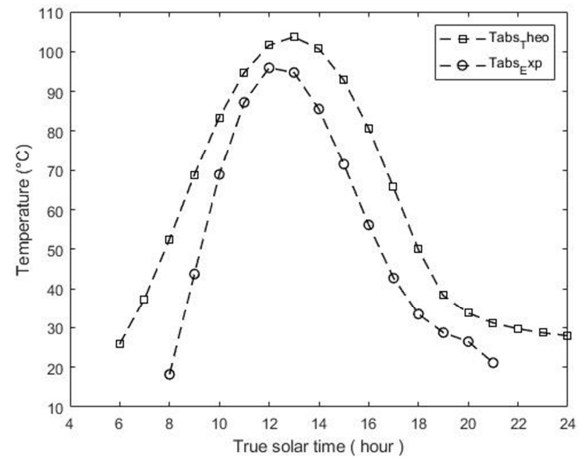


Figure 11. Comparison of experimental and simulated absorber temperature curve.

The values of R^2 obtained for the data of the solar radiation (Figure 9), collector outlet air temperature (Figure 10) and temperatures of the absorber (Figure 11) are respectively of the order of 0.960, 0.98 and 0.950, indicating a good correlation between the experimental and predicted data; whereas the root mean square error (RMSE) are respectively around 0.020, 0.013 and 0.011, showing a very good match between experimental and modeled temperatures.

4. Conclusions

In this work we were able to make a forced convection solar collector that could be applied in the future of drying. A physical and mathematical model followed by a simulation of the thermal behavior of the collector was developed. Following the simulation of the thermal behavior of the collector, experimental tests were carried out. The simulated temperatures, of the absorber, inlet air and outlet the collector during the course reach respectively the maximums values of the order of 105°C, 37°C and 92°C for solar irradiation maximum of 880 W/m². The maximum theoretical difference between the air temperature at the inlet and that at the collector outlet is around 55°C. This increment is fairly representative for the drying of local products. As for the experimental curves of the temperatures of the absorber, of the air inlet and outlet the collector of the same day, the values maximum are respectively of the order of 96°C, 78°C and 40°C for a maximum solar power of 900 W/m². The experimental temperature difference between the air inlet and outlet the collector during this test is therefore 38°C. The comparison between the simulated and experimental results revealed minor deviations due to climatic factors and experimental conditions. An in-depth study could be carried out to determine the instantaneous thermal efficiency of the collector as well as that of the coupling of the collector to a drying device.

Acknowledgements

This work was supported by the Ecole Normale Supérieure (ENS) as part of a call for projects (Decision n°2020_00062/MESRSI/SG/IDS/DG/SG/DAAS), year 2018, for the research professors of the Institute.

References

- [1] Plan national de développement économique et social (PNDES) 2016 2020, pp. 88, Burkina Faso, 2016.
- [2] N. K. Edem, B. BAMBARA, M. GAYE, Etude de marche solaire thermique: "production d'eau chaude et de séchage des produits agricole au Burkina Faso," Ouagadougou, pp. 64, 2015, <https://docplayer.fr/21109513-Burkina-faso-soltrain-afrique-d-e-l-ouestl.html>.
- [3] S. E. Tiendrebeogo, A. O Dissa, F. Cherblanc, I. Youm, J. C. Bénet, A. Compaoré, J. Koulidiati, "Characterization of Two Different Stumps of *Spirulina platensis* Drying: Assessment of Water Transport Coefficient," Food and Nutrition Sciences, Vol 6, pp. 1437-1449, 2015, <http://dx.doi.org/10.4236/fns.2015.615148>.
- [4] A. O Dissa, "Séchage convectif de la mangue: analyse de l'influence des paramètres aérauliques et intrinsèques, conception et modélisation du fonctionnement d'un séchoir solaire indirect," University of Ouagadougou No. d'ordre: 2007 / 048, pp 312, 2007.
- [5] I. G. Adamu, H. U. Kabri, I. D. Hussaini and A. D. Mada, "Design and construction of fish smoking kiln," Journal of Engineering and Technology Research, Vol. 5 (1), pp. 15-20, 2013, DOI: 10.5897/JETR-12-042.
- [6] T. Khaled, A. Khelifa, L. Boutina, I. Tabet, and S. Haddad, "Theoretical Study and Experimental Validation of Energetic Performances of Photovoltaic/Thermal Air Collector. International Journal of Photoenergy, Vol. 2018, pp. 10, 2018, <https://doi.org/10.1155/2018/2794068>.
- [7] V. Shemelin and T. Matuska, "Performance Modelling of Dual Air/Water Collector in Solar Water and Space Heating Application," International Journal of Photoenergy, Vol. 2019, pp. 10, 2019, <https://doi.org/10.1155/2019/8560193>.
- [8] A. Idlimam, A. Lamharrar, C. S. E. Kane, S. Akkad et M. Kouhila, "Etude expérimentale de la cinétique de séchage de l'écorce de grenadine dans un séchoir partiellement solaire en convection force," Revue des Energies Renouvelables, CER'07 Oujda pp. 237-240, 2007.
- [9] S. O. Amrouche and N. Benaouda, "Système de régulation d'un séchoir solaire pour plantes aromatiques et médicinales," Revue des Energies Renouvelables, SMSTS'08 Alger, pp. 221-228, 2008.
- [10] J. R. Puiggali and F. Penot, "Analyse du comportement dynamique et thermique d'un séchoir solaire constitué d'un capteur à matrice poreuse couplé à une cheminée solaire," Revue de Physique Appliquée, Vol. 18 (10), pp. 625-633, 1983, <http://dx.doi.org/10.1051/rphysap:019830018010062500>.
- [11] J. O. Almirón, M. A. Lara, "Experimental Development of Solar Collector of Unconventional Air," Sustainable Energy, Vol. 4, No. 1, 17-27, 2016, <http://dx.doi.org/10.12691/rse-4-1-3>.
- [12] N. M. Maundu, K. S. Kiptoo, K. Eliud, D. Kindole and Y. Nakajo, "Air-flow Distribution Study and Performance Analysis of a Natural Convection Solar Dryer," American Journal of Energy Research, Vol. 5, N°1, pp. 12-22, 2017, <http://dx.doi.org/10.12691/ajer-5-1-2>.
- [13] J. Yang, Q. Jiang, J. Hou and C. Luo, "A Study on Thermal Performance of a Novel All-Glass Evacuated Tube Solar Collector Manifold Header with an Inserted Tube," International Journal of Photoenergy, pp 7, Article ID 409517, 2015, <http://dx.doi.org/10.1155/2015/409517>.
- [14] Monsurat Bello, Matthew Olusola Oluwamukomi* and Victor N, "Enujuigha. Modeling of the adsorption isotherm of *Pleurotus ostreatus* using Guggenheim-Anderson-de Boer (GAB) equation," Journal of Engineering and Technology Research 11 (4): 41-46, 2019, <http://dx.doi.org/10.5897/JETR2017.0626>.
- [15] A. COMPAORE, "Etude énergétique d'un séchoir solaire hybride solaire-gaz: applications au séchage de l'oignon," Violet de Galmi". Thèse de doctorat, Université Ouaga 1, 156 p, ISBN 13: 978-620-2-28291-8, 2016.